

Basic e^+e^- Collider Physics

David L. Rubin

Cornell University, Ithaca, New York 14853, USA

In the most basic colliding beam storage ring bunches of counterrotating electrons and positrons share a common equilibrium orbit. The evenly spaced bunches collide at $2n_b$ locations around the ring, where n_b is the number of bunches in each beam. At each collision point the machine optics are manipulated to minimize both the spot size and the effect of the beam-beam interaction. The separated function guide field is characterized by alternate gradient focusing.

1 Equations of Motion

To the magnetic guide field there corresponds a Lorentz force

$$\mathbf{F} = q\mathbf{v} \times \mathbf{B} , \quad (1)$$

yielding identical trajectories for counterrotating and oppositely charge beams, at least in so far as the particle energy is independent of azimuthal location around the ring¹. Then the beam trajectories are described by the equation of motion

$$m \frac{d^2 \mathbf{x}}{dt^2} = q\mathbf{v} \times \mathbf{B} . \quad (2)$$

The field \mathbf{B} depends on the azimuthal position s along the magnetic axis of the machine. We define a cylindrical coordinate system in which x and y correspond to horizontal and vertical displacement with respect to the reference orbit. The reference orbit is circular. The radius of curvature is determined by the part of the field that is nonzero on the reference orbit, such as the uniform field of a bending magnet. The magnetic field can then be expanded about the reference

¹ Synchrotron radiation and RF acceleration both break the symmetry, leading to finite transverse displacement of the electron and positron orbits. The beams tend to have minimum energy at opposite ends of the accelerating cavities. Nevertheless, if the interaction points are located symmetrically with respect to the cavities, and if they are points of vanishing dispersion, head on collision of the electrons and positrons is certain.

orbit. If we define the coefficients of the terms linear in x and y as $k_x(s)$ and $k_y(s)$ respectively, the equations of motion become

$$\frac{d^2x}{ds^2} = k_x(s)x + F_x(s) \quad (3)$$

$$\frac{d^2y}{ds^2} = k_y(s)y + F_y(s) , \quad (4)$$

where the time t has been replaced by position along the trajectory s , as the dependent variable, and $k_x = -\frac{1}{R^2} + \frac{q}{\gamma mc} \frac{\partial B_y(0)}{\partial x}$ with $\frac{1}{R} = -\frac{q}{\gamma mc} B_y(0)$ and $k_y = -\frac{q}{\gamma mc} \frac{\partial B_x(0)}{\partial y}$. The functions $F_x(s)$ and $F_y(s)$ are meant to include all but the linear terms in the effective force. In the ideal linear lattice $F_x = F_y = 0$ [RW].

Then the change of variables:

$$x = \sqrt{\beta_x(s)} u_x \quad (5)$$

$$\phi(s) = \frac{1}{Q_x} \int^s \frac{ds'}{\beta_x(s')} , \quad (6)$$

yields

$$\frac{d^2 u_x}{d\phi^2} + Q_x^2 u_x = 0 , \quad (7)$$

and similarly for motion in the vertical direction. $\beta(s)$ is periodic in s , that is $\beta(s+C) = \beta(s)$, where C is the circumference of the machine and

$$2\pi \int_s^{s+C} \frac{ds'}{\beta_x(s')} = Q_x \quad (8)$$

so that ϕ advances from 0 to 2π in one full turn. The distribution of quadrupole magnets determines the frequency Q_x and Q_y of transverse oscillations.

There is of course a third such equation describing longitudinal or energy oscillations. The so-called synchrotron frequency depends on the time dependence of the accelerating voltage and the energy dependence of the revolution frequency.

1.1 Nonlinearities and Resonances

The field errors, magnetic nonlinearities, beam-beam interaction etc. are included in the term $F(s)$ which leads to the modification of the simple harmonic oscillations as follows:

$$\frac{d^2 u_x}{d\phi^2} + Q_x^2 u_x = Q_x^2 \beta_x^{3/2}(s) F_x(s) . \quad (9)$$

The driving term $F(s)$ is necessarily periodic in s and can be written as a Fourier expansion $F(s) \rightarrow \sum a_m e^{im\phi(s)}$. If for example the perturbing field is simply a

dipole kick sufficiently well localized that it can be described as a delta function, we can write, using (6),

$$F_x(s) = \delta(s)\Delta\theta = \frac{d\phi}{ds}\delta(\phi) = \frac{1}{Q\beta_x} \frac{\Delta\theta}{2\pi} \sum_{m=-\infty}^{\infty} e^{im\phi(s)} . \quad (10)$$

$\Delta\theta$ is the angular kick imparted to the beam by the dipole in question. Then (9) becomes

$$\frac{d^2u_x}{d\phi^2} + Q_x^2u_x = Q_x\beta_x^{1/2} \frac{\Delta\theta}{2\pi} \sum_{m=-\infty}^{\infty} e^{im\phi} \quad (11)$$

The driven oscillator (11) has resonances whenever $Q^2 - m^2 = 0$.

In general, in addition to its periodicity with respect to s , the function F may depend on the phase space coordinates of the particle $(x, x', y, y', l, \delta p/p)$. Such dependence leads to higher order resonances. For example, the force associated with a one dimensional, localized sextupole field is $F(x, s) = S(s)x^2$, where $S(s) = \frac{1}{2} \frac{\partial^2 B_y(s)}{\partial x^2} \frac{q}{\gamma mc}$. We suppose that the field is uniform over the length l of the magnet so that the net kick due to the sextupole is $\Delta\theta = Sx^2l$. If as before the s dependence is represented as a delta function, then the equation of motion is:

$$\frac{d^2u_x}{d\phi^2} + Q_x^2u_x = Q_x\beta_x^{1/2} \frac{Sx^2l}{2\pi} \sum_{m=-\infty}^{\infty} e^{im\phi} . \quad (12)$$

We solve for the motion perturbatively, replacing x by its unperturbed value namely $x = a\sqrt{\beta} \cos(Q_x\phi)$. Then (12) becomes

$$\frac{d^2u_x}{d\phi^2} + Q_x^2u_x = Q_x\beta^{3/2} \frac{a^2S}{2\pi} \frac{1}{2} \sum_{-\infty}^{\infty} [e^{i(m+2Q_x)\phi} + e^{i(m-2Q_x)\phi} + 2e^{im\phi}] . \quad (13)$$

The beam responds resonantly when $(m \pm 2Q)^2 - Q^2 = 0$, or when $Q = m/3$.

In general, if $F(s)$ is independent of x , resonances occur for $Q = m$. If $F(s, x) \sim x$ there are resonances whenever $Q_x = 2m$, and for $F(s, x) \sim x^2$ at $Q_x = 3m$ etc. For the most general case, the perturbation F , is a nonlinear function of x, y and z and the resonance condition is $pQ_x + rQ_y + nQ_z = m$ where p, r, n and m are integers. In an electron machine the radiation damping ameliorates the effects of all but relatively low order resonances. Nevertheless, great care is required in the choice of the operating point as we shall see.

1.2 Tune Plane

The resonant structure of the "tune plane" is apparent in a detailed measure of the beam lifetime, beam tails, or vertical beam size as a function of the machine tune. A simulated scan in the vicinity of the CESR operating point is shown in Figure 1. At each of 1600 tunes, we track a particle for 1000 turns. If the tunes are near a resonance condition, the amplitude will increase. We compute the maximum vertical amplitude of each particle. In CESR the revolution frequency

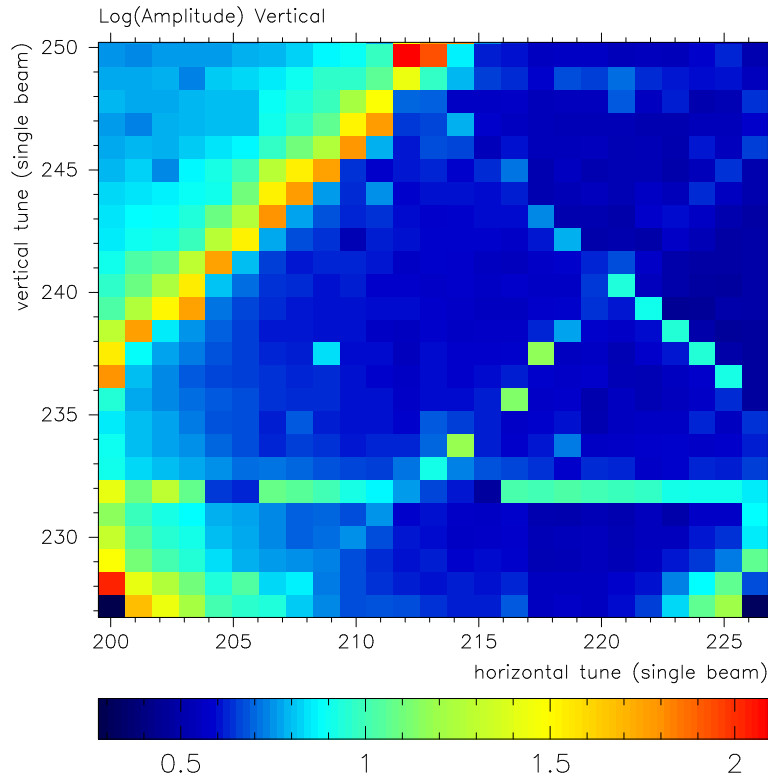


Fig. 1. Scan of vertical amplitude as a function of horizontal and vertical tune. The synchrotron tune $Q_s = -0.089$.

is 390.1kHz. The plotted range in horizontal tune is from $Q_x = 198.95/390.1$ to $226.26/390.1$, ($.51 < Q_x < .58$). The step size $\Delta f = 0.78\text{kHz}$ ($\Delta Q = 0.002$). The synchrotron tune $Q_s = -0.089$ is fixed throughout the scan. Resonance lines are identified on the companion plot Figure 2.

The coupling of the longitudinal and transverse motion appears in the scan as sidebands off of the horizontal half integer ($Q_x = .5$) and the transverse coupling resonance ($Q_x = Q_y$). The synchro-betatron coupling is due to the energy dependence of the optical functions² and/or the dispersion in the RF accelerating cavity. The dispersion is the energy dependence of the transverse displacement of the beam. Because the dispersion is nonzero in the CESR cavities, the RF kick, which also depends on energy, is coupled linearly to the horizontal displacement. Higher order transverse resonances are due to the cumulative effect of the machine sextupoles. Indeed, single beam resonance structure is well understood in terms of known coupling mechanisms and nonlinearities, and simulations yield

² The focusing function $k(s)$ that appears in equation (1) will in general depend on the beam energy and the beam energy oscillates at the synchrotron frequency.

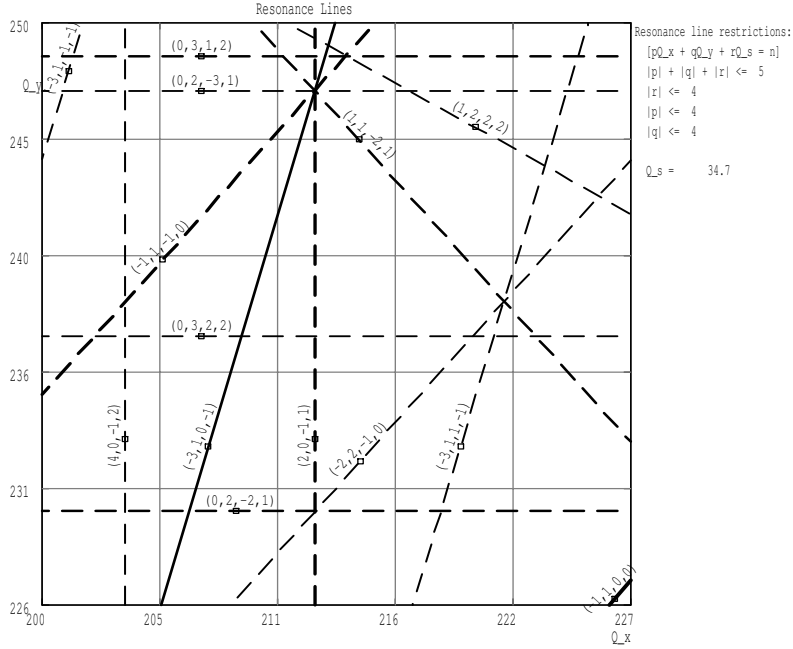


Fig. 2. Along each of the lines indicated in the plot the tunes satisfy a resonance condition $pQ_x + rQ_y + nQ_z = m$. The plot includes all lines for values $|p| + |r| + |n| \leq |5|$.

scans that bear a remarkable resemblance to the observed tune dependence of beam size shown in Figure 1.

1.3 Matrix Formalism

In view of (9) it is obviously of great interest to compute $\beta(s)$. In principle we might compute $\beta(s)$ by noting first of all that the solution to the homogenous equation of motion is $u_x = a \cos \phi$, where a is an arbitrary constant, and then that $x = a\sqrt{\beta} \cos \phi$. Then substitution into (3) and (4) with $F_x = F_y = 0$ and using (6), yields a differential equation for $\beta(s)$. Given the periodicity of $\beta(s)$, it is uniquely defined by the differential equation.

In practice it is more convenient to compute $\beta(s)$ by way of a matrix formalism. In so far as the guide field consists of distinct multipoles, the focusing function $k(s)$ in equations (3) and (4) is piecewise constant. That is, k is uniform through each quadrupole, bend and drift. Therefore (3) and (4) can be solved directly for the motion within each element. In particular

$$x(s) = A \cos(\sqrt{k}s) + B \sin(\sqrt{k}s) \quad (14)$$

$$x'(s) = -A\sqrt{k} \sin(\sqrt{k}s) + B\sqrt{k} \cos(\sqrt{k}s) . \quad (15)$$

The constants A and B are determined by specifying the values of x and x' at some s . If we write that $(x(0), x'(0)) = (x_0, x'_0)$ at the entrance to an element of length l then

$$x(l) = x_0 \cos(\sqrt{k}l) + \frac{x'_0}{\sqrt{k}} \sin(\sqrt{k}l) \quad (16)$$

$$x'(l) = -x_0\sqrt{k} \sin(\sqrt{k}l) + x'_0\sqrt{k} \cos(\sqrt{k}l) , \quad (17)$$

and in matrix notation:

$$\begin{pmatrix} x(l) \\ x'(l) \end{pmatrix} = M \begin{pmatrix} x_0 \\ x'_0 \end{pmatrix} = \begin{pmatrix} \cos(\sqrt{k}l) & \frac{1}{\sqrt{k}} \sin(\sqrt{k}l) \\ -\sqrt{k} \sin(\sqrt{k}l) & \cos(\sqrt{k}l) \end{pmatrix} \begin{pmatrix} x_0 \\ x'_0 \end{pmatrix} . \quad (18)$$

Each linear machine element can be described by a similar unit determinant matrix, and the mapping of the phase space vector (x, x') through a sequence of elements, by the product of the intermediate matrices.

Now consider propagation of the vector[CS1]

$$\mathbf{x}_1 \rightarrow \mathbf{x}_2 = M\mathbf{x}_1 , \quad (19)$$

where $x_1 = a\sqrt{\beta_1} \cos \phi_1$. Differentiation with respect to s yields $x'_1 = a\frac{1}{2}\frac{\beta'_1}{\sqrt{\beta_1}} \cos \phi_1 - a\frac{1}{\sqrt{\beta_1}} \sin \phi_1$. Then equation (18) becomes:

$$\begin{pmatrix} a\sqrt{\beta_2} \cos \phi_2 \\ -a\frac{\alpha_2}{\sqrt{\beta_2}} \cos \phi_2 - a\frac{1}{\sqrt{\beta_2}} \sin \phi_2 \end{pmatrix} = M \begin{pmatrix} a\sqrt{\beta_1} \cos \phi_1 \\ -a\frac{\alpha_1}{\sqrt{\beta_1}} \cos \phi_1 - a\frac{1}{\sqrt{\beta_1}} \sin \phi_1 \end{pmatrix} . \quad (20)$$

Note that we have defined $\alpha \equiv -\frac{1}{2}\beta'$. Now if we define the matrix

$$G_i = \begin{pmatrix} \sqrt{\beta_i} & 0 \\ -\frac{\alpha_i}{\sqrt{\beta_i}} & -\frac{1}{\sqrt{\beta_i}} \end{pmatrix} \quad (21)$$

so that

$$\begin{pmatrix} x \\ x' \end{pmatrix} = G \begin{pmatrix} \cos \phi \\ \sin \phi \end{pmatrix}, \quad (22)$$

then (20) can be rewritten in a most suggestive form, namely

$$G_2 \begin{pmatrix} a \cos \phi_2 \\ a \sin \phi_2 \end{pmatrix} = MG_1 \begin{pmatrix} a \cos \phi_1 \\ a \sin \phi_1 \end{pmatrix} . \quad (23)$$

Apparently

$$G_2^{-1}MG_1 = \begin{pmatrix} \cos \Delta\phi & -\sin \Delta\phi \\ \sin \Delta\phi & \cos \Delta\phi \end{pmatrix}. \quad (24)$$

Here $\Delta\phi = \phi_2 - \phi_1$. Finally, (24) can be solved for M , and M can be written in terms of the twiss parameters α , β , and ϕ ³.

$$\begin{aligned} M &= G_2 \begin{pmatrix} \cos \Delta\phi & \sin \Delta\phi \\ -\sin \Delta\phi & \cos \Delta\phi \end{pmatrix} G_1^{-1} \\ &= \begin{pmatrix} \sqrt{\frac{\beta_2}{\beta_1}}[\cos \Delta\phi + \alpha_1 \sin \Delta\phi] & \sqrt{\beta_2\beta_1} \sin \Delta\phi \\ \frac{1}{\sqrt{\beta_1\beta_2}}[\Delta\alpha \cos \Delta\phi - (1 + \alpha_2\alpha_1) \sin \Delta\phi] & \sqrt{\frac{\beta_1}{\beta_2}}[\cos \Delta\phi - \alpha_2 \sin \Delta\phi] \end{pmatrix}, \end{aligned} \quad (25)$$

where $\Delta\alpha = \alpha_1 - \alpha_2$. And if M is the full turn matrix, then $\beta_1 = \beta_2 = \beta$, $\alpha_1 = \alpha_2 = \alpha$ and $\Delta\phi = \mu = 2\pi Q$, and

$$M(s+C, s) = \begin{pmatrix} \cos \mu + \alpha \sin \mu & \beta \sin \mu \\ -\gamma \sin \mu & \cos \mu - \alpha \sin \mu \end{pmatrix}. \quad (26)$$

($\gamma \equiv (1 + \alpha^2)/\beta$.) The twiss parameters at any point in the machine are thus determined by computation of the full turn transfer matrix at that point.

1.4 Propogating Twiss Parameters

The reader may be amused by a further extension of the formalism that permits propogation of the twiss parameters through a sequence of elements. Returning to (22), it is clear that for any phase space vector $\mathbf{x} = (x, x')$ that $G^{-1} \begin{pmatrix} x \\ x' \end{pmatrix} = a \begin{pmatrix} \cos \phi \\ \sin \phi \end{pmatrix}$ so that the quantity $(G_{11}^{-1}x + G_{12}^{-1}x')^2 + (G_{21}^{-1}x + G_{22}^{-1}x')^2 = a^2(\cos^2 \phi + \sin^2 \phi)$ is an invariant. Substitution of the elements of G^{-1} identified in (21), yields $a^2 = \gamma x^2 + 2\alpha x x' + \beta x'^2 \equiv \boldsymbol{\gamma} \cdot \mathbf{X}$ where the three vectors $\boldsymbol{\gamma} = (\gamma, 2\alpha, \beta)$ and $\mathbf{X} = (x^2, x x', x'^2)$. The scalar product is an invariant. Since we know how x and x' propogate we can construct a 3×3 matrix \mathcal{M} corresponding to propogation of \mathbf{X} . The reader can verify that

$$\mathcal{M} = \begin{pmatrix} M_{11}^2 & 2M_{11}M_{12} & M_{12}^2 \\ M_{11}M_{21} & (M_{11}M_{22} + M_{12}M_{21}) & M_{12}M_{22} \\ M_{21}^2 & 2M_{21}M_{22} & M_{22}^2 \end{pmatrix}. \quad (27)$$

Then $\mathbf{X}_2 = \mathcal{M}\mathbf{X}_1$. We would like to determine the corresponding matrix \mathcal{N} for $\boldsymbol{\gamma}$. Since $\boldsymbol{\gamma}_2 \cdot \mathbf{X}_2 = \boldsymbol{\gamma}_1 \cdot \mathbf{X}_1 = \boldsymbol{\gamma}_1 \cdot \mathcal{M}^{-1}\mathcal{M}\mathbf{X}_1 = \boldsymbol{\gamma}_1 \mathcal{M}^{-1}\mathbf{X}_2$, it is obvious that

³ Note that for a 2×2 matrix T , $T^{-1} = T^\dagger / \det T$ and if $T = \begin{pmatrix} a & b \\ c & d \end{pmatrix}$, then $T^\dagger = \begin{pmatrix} d & -b \\ -c & a \end{pmatrix}$.

$\gamma_2 = (\mathcal{M}^{-1})^T \gamma_1$ and $\mathcal{N} = (\mathcal{M}^{-1})^T$. \mathcal{N} is constructed by replacing the elements of M with those of its inverse in (28) and transposing, yielding⁴

$$\mathcal{N} = \begin{pmatrix} M_{22}^2 & -M_{22}M_{21} & M_{21}^2 \\ -2M_{22}M_{12} & (M_{11}M_{22} + M_{12}M_{21}) & -2M_{21}M_{11}^2 \\ M_{12}^2 & -M_{12}M_{11} & M_{11}^2 \end{pmatrix}. \quad (29)$$

As an example consider the propagation of the twiss parameters through a field free region. Using (18) to obtain the elements of the matrix M through the field free region we find that

$$\mathcal{N}(s) = \begin{pmatrix} 1 & 0 & 0 \\ -2s & 1 & 0 \\ s^2 & -s & 1 \end{pmatrix}. \quad (30)$$

At a point of minimum β , in a field free region, like that near the interaction point, $\gamma_0 = (1/\beta_0, 0, \beta_0)$ and at a distance s from the minimum,

$$\gamma(s) = \mathcal{N}\gamma(0) = (1/\beta_0, -2s/\beta_0, \beta_0 + s^2/\beta_0). \quad (31)$$

2 Luminosity

The objective of the basic collider is of course, luminosity which depends on the beam parameters as:

$$L = \frac{n_b f_{rev} N_b^2}{4\pi \sigma_x \sigma_y}. \quad (32)$$

n_b is the number of bunches, N_b the number of particles per bunch, f_{rev} the revolution frequency and σ_x and σ_y the transverse beam size at the collision point. That is as long as the bunch length is small compared to height and/or width. It is clear that for a given beam current, L is a maximum when the cross sectional area of the bunch is a minimum. The minimum bunch size is limited by the beam-beam interaction.

2.1 Beam-Beam Interaction

The dependence of the vertical kick experienced by a particle in one beam, as a function of its displacement from the centroid of the opposing beam is indicated in Figure 3. The force is linear in displacement as long as that displacement is small, giving rise to the linear beam-beam tune shift. The focal length associated with the presumed gaussian charge distribution in the linear regime is:

$$\frac{1}{f_i} = \frac{2N_b r_e}{\gamma(\sigma_x + \sigma_y)\sigma_i}, \quad (33)$$

⁴ In the case of coupled motion with transport described by 4×4 matrices, the procedure is readily generalized. γ becomes a 10 component vector and \mathcal{N} a 10×10 matrix.

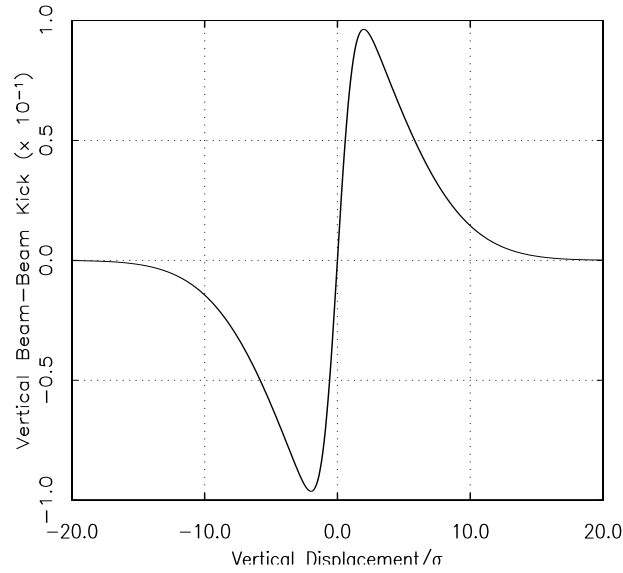


Fig. 3. The vertical beam-beam kick as a function of vertical displacement from the center of the opposing bunch for an aspect ratio $\sigma_x/\sigma_y = 10$. The kick is in arbitrary units and the displacement in units of the rms vertical beam size.

where $i = x, y$ and r_e is the classical radius of the electron. And the corresponding beam-beam tune shift is

$$\Delta Q_i = \frac{\beta_i^*}{4\pi f_i} . \quad (34)$$

The field becomes increasingly nonlinear for $y \geq \sigma_y$. The beam-beam interaction is the most important source of nonlinearity in the machine, or at least it should be. Presumably it is the nonlinearities that will limit the luminosity per unit current. Machine nonlinearities, that is, sextupole induced nonlinearities can be controlled by careful design. The beam-beam induced nonlinearities are beyond our control. Let us consider some of the dynamical implications of the beam-beam interaction.

2.2 Beam-beam coupling

In the event of counterrotating beams in collision we need to write an equation of motion for each. The resulting coupled equations are:

$$\frac{d^2 u_1}{d\phi^2} + Q_1^2 u_1 = Q_1^2 \beta^{*\frac{3}{2}} F_2(x_1 - x_2) \quad (35)$$

$$\frac{d^2 u_2}{d\phi^2} + Q_2^2 u_2 = Q_2^2 \beta^{*\frac{3}{2}} F_1(x_2 - x_1) . \quad (36)$$

u_1 and u_2 are horizontal coordinates for the motion of beams 1 and 2 respectively. F_1 is the force on beam 2 due to beam 1 and F_2 the force on beam 1 due to beam 2. The beam beam coupling yields normal modes A and B with tunes Q_A and Q_B such that $Q_A - Q_B \propto \Delta Q$, with ΔQ given in (34). In the limit of a purely linear beam-beam kick, the coupled equations can be solved by making the substitution $u_1 = u_A + u_B$ and $u_2 = u_A - u_B$. Then the tune of mode, A, the σ mode is the same as the unperturbed tune Q , and mode B, the π mode is shifted such that $Q_B - Q_A = 2\Delta Q$, for ΔQ defined above. That is, the normal mode splitting is just twice the linear beam-beam tune shift.

The beam-beam coupling can also be evaluated in a matrix formalism. In the absence of the beam-beam coupling, the phase space coordinates x and x' are mapped through a single turn by a 2×2 matrix M , so that $\mathbf{x}_{n+1} = M\mathbf{x}_n$ and $\mathbf{x} = (x, x')$. If the eigenvalues λ , of M have unit magnitude, then the motion is stable. The eigenvalues have the form $\lambda = e^{\pm i\mu}$ and the tune $Q = \mu/2\pi$.

In order to add the linear beam-beam coupling we need to generalize the phase space vector to accomodate the coordinates of both beams. So we define $\mathbf{X} = (x_1, x'_1, x_2, x'_2)$, where subscripts 1 and 2 indicate beams 1 and 2 respectively. Then propagation through a full turn is described by the 4×4 matrix $T = \begin{pmatrix} M & 0 \\ 0 & M \end{pmatrix}$. The beam-beam kick is given by the

$$B = \begin{pmatrix} C & D \\ D & C \end{pmatrix} = \begin{pmatrix} 1 & 0 & 0 & 0 \\ 1/f & 1 & -1/f & 0 \\ 0 & 0 & 1 & 0 \\ -1/f & 0 & 1/f & 1 \end{pmatrix} . \quad (37)$$

Then according to B , the kick received by beam 1 is $\Delta x'_1 = (x_1 - x_2)/f$, etc. and f is the focal length given above. The full turn matrix

$$F = BT = \begin{pmatrix} CM & DM \\ DM & CM \end{pmatrix} \quad (38)$$

and the eigenvalues of F yield the normal mode tunes. In particular

$$\cos \mu_A - \cos \mu_B = [(\cos \mu_1 - \cos \mu_2)^2 + |DM + (DM)^\dagger|]^{\frac{1}{2}} . \quad (39)$$

The technique is readily generalized to include the effects of multiple beam-beam interactions in a single turn. Of course the beam-beam kick is linear only over a rather limited range. For particles with amplitudes that sample the nonlinear

fields of the opposing bunch, the kick falls rapidly with displacement and the measured normal mode splitting is somewhat less than that predicted by the purely linear model.[SM1][CBW1] Apparently the region of the tune plane clear of resonances must expand with the beam-beam interaction to accomodate the splitting of the normal modes.

2.3 Saturation of the Tune Shift Parameter

In the limit where $\sigma_y \ll \sigma_x$ the beam-beam tune shift parameter

$$\xi_v \equiv \Delta Q = \frac{\beta^*}{2\pi} \frac{2I_b r_e}{e f_{rev} \sigma_x \sigma_y} \quad \text{and} \quad L = \frac{n_b \gamma I_b \xi_v}{2\beta^* e r_e} . \quad (40)$$

I_b is the bunch current, e the charge of the electron, and we have made use of (32-34). The strength of the beam-beam interaction increases with bunch current, as the charge per unit area of the bunch. Resonant response of one beam to the other eventually leads to an increase in the area of the bunch that precludes further growth of the bunch charge density. The tune shift parameter is saturated. Beyond saturation luminosity increases linearly with current. The maximum luminosity per unit current obtains above saturation and so that is clearly the regime in which to operate.[JS1] It is evidently desirable to remain in saturation throughout the course of a fill. Data collected at the Cornell Electron Storage Ring operation for high energy physics, and shown in Figures 4 and 5, indicate both saturation of the tune shift parameter and the linear dependence of luminosity on current.

2.4 Minimum β

It should be apparent from the foregoing discussion, that in order to achieve maximum luminosity it is sensible to minimize β^* , that is β at the interaction point, to maximize the beam current, and to maximize the value of the saturated tune shift parameter. We consider the three variables in turn.

There are two reasons why it is attractive to make β^* as small as possible. We see from the equations of motion that the effects of the beam-beam interaction scale with β at the collision point. Also the beam size scales inversely with $\sqrt{\beta^*}$.

One of the limitations to β^* from below is related to the finite bunch length. Near the minimum $\beta(s) = \beta_0 + \frac{s^2}{\beta_0}$, (see equation (31)), where β_0 , is the minimum and s the distance from the minimum. If the bunch length $\sigma_z \sim \beta_0$, then there will be a significant increase in the effective β of the interaction as compared to the minimum value. In practice β^* can be no smaller than the the length of the bunch.

It is also apparent from the quadratic growth near the IP that if β^* is very small that either β is very large in the final focus quadrupoles, or the quadrupoles are very strong and very near to the interaction point. Both scenarios contribute

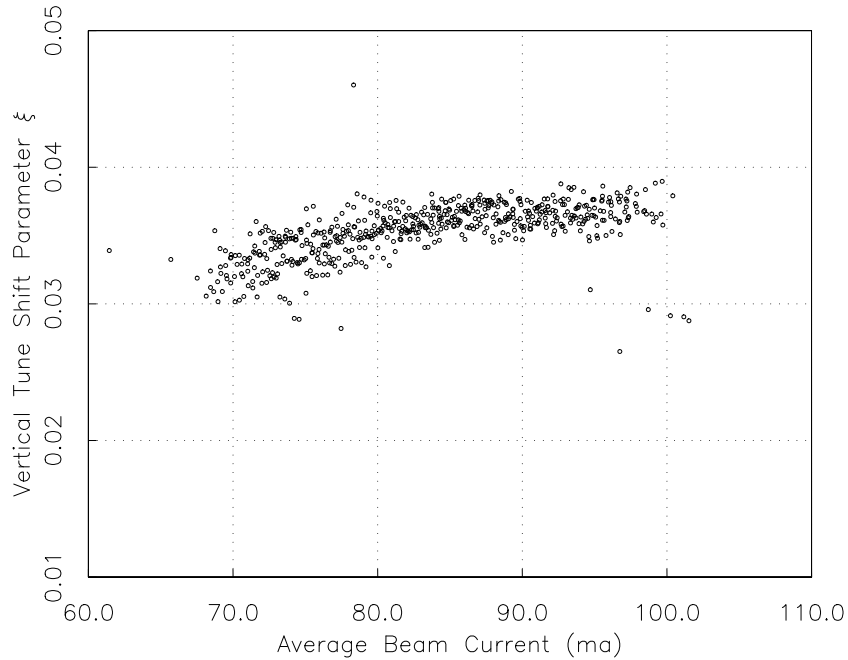


Fig. 4. Beam-beam tune shift parameter as a function of average beam current. There are seven bunches in each beam. Data collected during a 24 hour period of operation for high energy physics is shown.

to the chromaticity of the machine and the demand for stronger sextupole magnets. And as noted above, sextupole fields drive all manner of nonlinear resonances. Also, the interaction region tends to be cluttered with particle detectors and there is not always adequate real estate for optimal placement of such quadrupoles.

There are other practical, rather than fundamental limits on the minimum β . Consider for a moment the possibility that the collision point is displaced longitudinally with respect to the focal point. Then the beams interact with each other in a region in which β may be changing rapidly over the length of the bunch. Again, the rate of change of β scales with $\frac{1}{\beta_0}$, and so does the sensitivity to such longitudinal alignment errors. In the basic single ring collider, the collision point, that is the point at which counterrotating bunches arrive simultaneously, is determined by the physical location and relative phase of the RF cavities. In the simplest case, in which there is a single cavity, the difference between the arrival time of the electron and positron bunches in the cavity is an integral number of RF periods. In order that the bunches arrive simultaneously at the beta minimum, the distance from cavity to that minimum must be an integral number of RF wavelengths. For $\beta^* \sim 1\text{cm}$, alignment to a few millimeters is required.

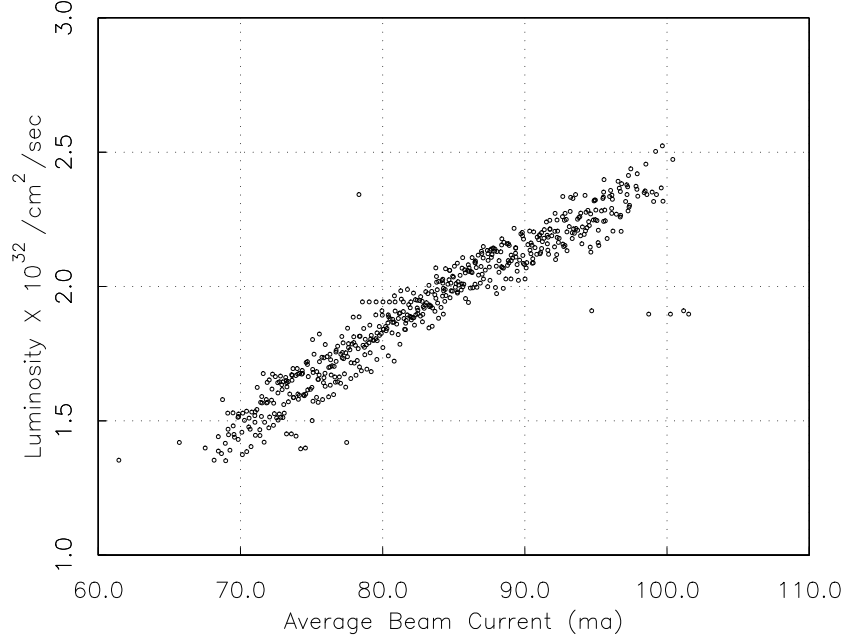


Fig. 5. Luminosity as a function of average beam current.

At CESR, with $\beta^* = 1.8$ and $\sigma_l \sim 1.9\text{cm}$ a beam-beam tune shift limit of $\Delta Q_v \sim 0.04$ is measured. In experimental optics designed to both shorten the bunch and reduce β^* to 1.3cm , we measure $\Delta Q_v \sim 0.03$. Finally for $\beta^* \sim 10\text{cm}$ and $\sigma_l = 1.9\text{cm}$, $\Delta Q_v \sim 0.06$.

2.5 Increasing the Beam-Beam Limit

Referring again to our expression for luminosity (40), it is clear that maximizing the limiting beam-beam tune shift is of great interest. Our discussion of beam-beam coupling suggested that nonlinear resonances are largely responsible for limiting the bunch charge density, and that the beam-beam interaction itself is the source of many such resonances. In the basic collider with a single bunch in each beam, the counterrotating bunches collide at two diametrically opposed points. The equation of motion including the effects of the beam-beam interaction at both points is:

$$\frac{d^2u}{d\phi^2} + Q^2 = Q^2 \beta(s)^{\frac{3}{2}} (f_1(\mathbf{x}_1, s_1) + f_2(\mathbf{x}_2, s_2)) . \quad (41)$$

Taking advantage of the periodicity in s we have:

$$\frac{d^2u}{d\phi^2} + Q^2 = Q^2 \beta(\phi)^{\frac{3}{2}} \left(\sum_m a_m^1(\mathbf{x}) e^{im(\phi-\phi_1)} + \sum_m a_m^2(\mathbf{x}) e^{im(\phi-\phi_2)} \right) . \quad (42)$$

If the twiss parameters at the two collision points are identical, $f_1 = f_2$, and $a_m^1 = a_m^2 = a_m$

$$\frac{d^2u}{d\phi^2} + Q^2 = Q^2 \beta(\phi)^{\frac{3}{2}} \sum_m a_m(\mathbf{x}) e^{im\phi} \left(e^{-im(\phi_1 + \phi_2)} \right) \quad (43)$$

$$= Q^2 \beta(\phi)^{\frac{3}{2}} \sum_m a_m(\mathbf{x}) e^{im\phi} e^{-i\frac{m}{2}\phi^+} 2 \cos \frac{m}{2}\phi^- , \quad (44)$$

where $\phi^\pm = \phi_1 \pm \phi_2$. If the betatron phase advance separating the points is identically $2\pi(Q/2)$ then $\phi^- = \phi_1 - \phi_2 = \pi$. All m odd terms vanish and m even terms increase by a factor of two. The resonance condition is $pQ = 2m$. We might equivalently imagine that a single turn of the machine is two turns of a simpler machine with tune $Q \rightarrow Q_{\frac{1}{2}} = Q/2$. In the smaller machine there is a single beam-beam interaction with resonances at all m , $pQ_{\frac{1}{2}} = m$. It is easy to show with the help of (43,44) that for each resonance $pQ = 2m$ that there is a corresponding resonance $pQ_{\frac{1}{2}} = m$ of equal strength. In such an idealized case of symmetrically placed collision points, the resonance behavior is determined not by the full turn phase advance but rather by the phase advance from one point to the next, that is by $Q_{\frac{1}{2}}$. Multiple collision points are in such circumstance no cause for alarm as long as the point $Q_x/N, Q_y/N$ in the tune plane is clear of dangerous resonances. N is the number of interaction points per turn.

In practice it is very difficult to achieve perfect symmetry, both in terms of phase advance and interaction point parameters. Furthermore, resonances are excited by machine hardware, such as RF cavities and sextupole magnets. All such hardware must be symmetrically placed in order to ensure that $Q_{\frac{1}{2}}$ and not Q determine the resonance behavior. As an example, suppose that there are two interaction points and only a single RF cavity. Synchro-betatron resonances associated with cavity field nonlinearities will be circumscribed by the full turn tune. Beam-beam resonances will depend on the half turn tune. While it may be desirable to operate with phase advance just above the half integer for best beam-beam performance, in a machine with two interaction points that implies a full turn tune just above the integer, very near to the synchro-betatron coupling resonance.

We conclude that while in principle performance is very nearly independent of numbers of collision points, the requisite optical symmetry is difficult to achieve and at very least is an expensive constraint on the machine design. The result of asymmetries is excitation of additional resonances and the narrowing of available good operating regions of the tune plane, and ultimately reduced beam-beam tune shift. Of course it is also much easier to keep one group of experimentalists happy than two.

In so far as radiation damping determines the equilibrium beam size it is desirable to have fewer collision points. The radiation damping decrement δ , is the ratio of the time between collisions to the radiation damping time. A machine with one rather than two beam-beam collisions per turn has twice the damping decrement between collisions. On the other hand, that decrement is typically of

order one part in 10^4 and it is not clear how a factor of two is relevant. There is however some evidence that the limiting tune shift parameter $\xi_v \sim \sqrt{\delta}[\text{JS1}]$ [R1].

2.6 Multiple Bunches

Luminosity is expected to scale with the number of bunches in each beam at fixed bunch current. As noted above, the number of collision points in the ring is twice the number of bunches in the beam. And there can be no longer any doubt that the consequence of those parasitic collisions will be a degradation of the beam-beam limiting tune shift. At best we suffer for having complicated the tune-plane. And unless we are prepared to install a low beta insert at each of the new crossing points, the beam-beam current limit will fall precipitously. It is therefore attractive to consider separation of the beams at the parasitic crossing points, and this is typically accomplished with electrostatic deflectors. The most straightforward implementation is to locate separators $\pm\frac{1}{4}$ wavelengths from the crossing point, generating a half wavelength closed bump. Since the beam width tends to be many times the beam height, separation based on beam size is simpler in the vertical than in the horizontal plane. For the same reason, it is somewhat easier to build vertical than horizontal separators. The disadvantage of vertical separation is that vertical displacement in sextupole magnets introduces transverse coupling. If the vertical displacement is opposite for the two beams, then the transverse coupling is differential and therefore difficult to correct. Vertical separation is most usefully employed in regions devoid of sextupoles.

As the number of bunches in each beam, and the number of parasitic crossing points is increased, it is advantageous to generate with a minimal set of electrostatic deflectors, a differential closed orbit distortion that yields separation at multiple crossing points. In the "pretzel" scheme the closed orbits are off axis through a large fraction of the machine arcs and the sextupole induced coupling noted above renders vertical separation a dubious proposition. At CESR, two symmetrically placed and powered pairs of horizontal deflectors, separate the seven bunch beams at the thirteen parasitic crossing points as shown in Figure 6.

Optical Effects of Differential Displacement in Quadrupoles. Because the orbits of the electrons and positrons are distinct through most of the quadrupole magnets, and nearly all of the nonlinear elements in the storage ring, there will in general be differences in the electron and positron beam parameters that increase with separator voltage. The exclusive use of magnetic elements for the guide field in the simplest machine assured commonality of closed orbits and beam optics. The introduction of the differential distortion by way of electrostatic elements spoils that symmetry and it is compensated only by employment of specific design criteria.

In general both quadrupole and sextupole magnets can contribute to differences in the characteristics of the off axis electron and positron beams. The effective field of a quadrupole magnet on the closed orbit is that of a bend with

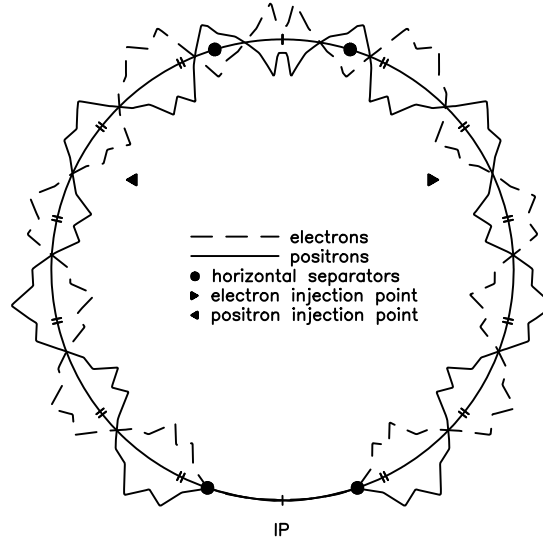


Fig. 6. Electron and positron closed orbits are designed to separate the beams at the parasitic crossing points that arise with seven bunches in each beam. The crossing points are indicated by the tick marks in the plot. Multiple crossing points within a lobe of the orbit arise due to the unequal bunch spacing.

radius of curvature inversely proportional to the displacement. Electrons and positrons thus experience equal but opposite fields, and there will be asymmetric contributions to the dispersion function.

The radiation damping times will also be different for electrons and positrons. The damping rate α_E for energy oscillations is determined by the dependence of the rate at which energy is radiated on the energy itself. That is $\alpha_E = \frac{1}{T_0} \frac{dU_{rad}}{dE}$ where T_0 is the revolution period and U_{rad} is the synchrotron radiated energy[S1] In addition to the fact that U_{rad} depends as the square of the energy there are contributions related to the dependence of the closed orbit on the energy. In a dipole magnet in which there is positive dispersion, the trajectory of higher energy particles is at a larger radius than that of lower energy particles. The higher energy particles therefore spend more time in the bend field and radiate more energy. Now imagine a beam with closed orbit displace in a quadrupole. Suppose that it is in a region of positive dispersion. If the displacement is towards the outside of the ring then the higher energy particles in the beam will be displaced even further away from the axis of the quadrupole and will radiate more than the lower energy particles. On the other hand, if the beam is displaced toward the inside of the ring, the higher energy particles will still be displaced

toward the outside and in this case that means closer to the quad axis. The higher energy particles then radiate less than the lower energy particles, contributing an anti-damping component. Quantitatively $\alpha_E = \frac{U_0}{2T_0 E_0} (2 + \mathcal{D})$ where

$$\mathcal{D} = \frac{\oint \eta G (G^2 + 2k) ds}{\oint G^2 ds} , \quad (45)$$

$G(s) = 1/\rho(s)$ and $\rho(s)$ is the radius of curvature of the on energy particle in the dipole field and k is defined in (3) and (4). In the event of displaced orbits in quadrupoles $\rho(s) = \frac{1}{x(s)k(s)}$ and (45) becomes

$$\mathcal{D} = \frac{\sum_i \eta_i (G_i^3 + 2x_i k_i^2) l_i}{\sum_i (G_i^2 + (x_i k_i)^2) l_i} \quad (46)$$

where the integral is replaced by a sum over discrete elements and l_i is the length of each. To lowest order, neglecting the dependence of the dispersion on the particle species and noting that $x_i^+ = -x_i^-$,

$$\mathcal{D}_+ - \mathcal{D}_- = \frac{2 \sum_i \eta_i (2x_i k_i^2) l_i}{\sum_i G_i^2 l_i} . \quad (47)$$

Since the damping of the longitudinal oscillations is different for electrons and positrons, so is the damping of horizontal oscillations. As a consequence of the differences in damping times and dispersion the beam emittances will be distinct.

Effects of Differential Displacement in Sextupole Fields. The differential displacement of the beams in the sextupoles is perhaps even more serious than in the quadrupoles. A sextupole behaves like a quadrupole with focal length inversely proportional to the displacement from the axis. The quadrupole distribution determines the β function and the tune. Electrons and positrons may well have different tunes and β^* in a machine with pretzeled orbits. Sometimes it is possible to eliminate differential effects by exploiting various symmetries. In CESR for example, which is symmetric about the diameter that includes the interaction point, an antisymmetric closed orbit distortion yields equal tunes and emittances and β^* , but in general unequal dispersion and $\beta(s)$ throughout the arcs and nonzero β' at the interaction point.

Evaluation of Optical Parameters of Displaced Beams. In any event, the optics can be designed to minimize the electron and positron differences as long as we know how to calculate those differences, and it is to that end that we now turn our attention. We showed earlier the relationship between the elements of the linear map and the twiss parameters, β, β' and the phase advance ϕ . If the closed orbit is coincident with the longitudinal axis of the machine elements, then the full turn linear map is simply the product of the individual linear transfer matrices. Remember that for nonlinear elements such as sextupoles the

linear part of the transfer matrix is simply that of a field free region. The matrix describes the linear dependence of the phase space coordinates of the trajectory as it leaves the element, on the phase space coordinates at its entrance.

In a nonlinear element the linear part of the mapping of the phase space will in general depend on the displacement of the trajectory from the magnetic axis. Therefore the linear part of the mapping depends on the closed orbit. We can compute the linear part of the mapping, that is the Jacobian of the map, but first we must identify the coordinates of the closed orbit.

If we write the dependence of phase space coordinates of the trajectory as it exits the magnet or sequence of magnets on the initial coordinates as $x_i^{out}(x_j^{in})$ then the Jacobian

$$J_{ij} = \frac{\partial x_i^{out}}{\partial x_j^{in}} . \quad (48)$$

Here x_i^{out} and x_j^{in} refer to the displacements $x, x', y, y' \dots$ from the closed orbit. If all of the machine elements are strictly linear then $J_{ij} = M_{ij}$ where M is the product of the individual transfer matrices. In the presence of nonlinear elements, the derivatives, J_{ij} can be computed numerically with a tracking code. If the mapping is through a full turn then there exists a closed orbit and its coordinates can be computed as well. If the motion is confined to a plane, so that $\mathbf{x} = (x, x')$, then it is necessary to compute $\Delta \mathbf{x}^{out}$ as a function of three distinct initial values $\Delta \mathbf{x}^{in}$ to establish both the location of the closed orbit and the matrix J . This is accomplished by tracking from the phase space coordinate $\mathbf{x}_0 + \Delta \mathbf{x}^{in}$ through the full turn to find $\mathbf{x}_0 + \Delta \mathbf{x}^{out}$. \mathbf{x}_0 is the coordinate of the closed orbit. The numerically computed Jacobian is the Jacobian of partial derivatives in the limit where $\Delta \mathbf{x}^{in} \rightarrow 0$. Since $\Delta \mathbf{x}^{in}$ is the displacement with respect to the closed orbit and the closed orbit is in general not well established a priori, iteration may be required to obtain sufficient accuracy.

For motion that may include transverse coupling $\mathbf{x} = (x, x', y, y')$, five distinct trajectories establish the 4×4 Jacobian matrix and the closed orbit. In order to determine the linear full turn map we suppose that initial and final coordinates are related as follows

$$\begin{aligned} \Delta \mathbf{x}_\alpha^{out} &= J \Delta \mathbf{x}_\alpha^{in} & (49) \\ &= \mathbf{x}_\alpha^{out} - \mathbf{x}^0 = J(\mathbf{x}_\alpha^{in} - \mathbf{x}^0) . & (50) \end{aligned}$$

Then

$$\mathbf{x}_\alpha^{out} = J \mathbf{x}_\alpha^{in} - (J - I) \mathbf{x}_\alpha^0 = J \mathbf{x}_\alpha^{in} + \mathbf{z}^0 , \quad (51)$$

where $\mathbf{z}^0 = (I - J) \mathbf{x}^0$. The suffix α runs from one to five and indicates the five initial sets of coordinates x_α^{in} mapped to the five final vectors x_α^{out} , and $x_{i\alpha}^{out}$ indicates the i^{th} component of the α^{th} vector. That is $x_{i\alpha}^{out} = J_{ij} x_{j\alpha} + z_j^0$. Now define the matrices

$$Y = \begin{pmatrix} x_{11} & x_{12} & x_{13} & x_{14} & x_{15} \\ x_{21} & x_{22} & x_{23} & x_{24} & x_{25} \\ x_{31} & x_{32} & x_{33} & x_{34} & x_{35} \\ x_{41} & x_{42} & x_{43} & x_{44} & x_{45} \\ 1 & 1 & 1 & 1 & 1 \end{pmatrix} , \quad (52)$$

and

$$H = \begin{pmatrix} & & & & -z_1^0 \\ & & & & -z_2^0 \\ & & & & -z_3^0 \\ & & & & -z_4^0 \\ 0 & 0 & 0 & 0 & 1 \end{pmatrix}, \quad (53)$$

so that (51) becomes

$$Y^{out} = HY^{in}. \quad (54)$$

Then $H = Y^{out}[Y^{in}]^{-1}$ from which the Jacobian and the coordinate of the closed orbit can be extracted [SB1]. The twiss parameters in turn are defined by the Jacobian. Once the closed orbit has been established the linear mapping between any two points in the lattice can be calculated in this fashion, yielding $\beta(s)$ and $\phi(s)$ along the trajectory of the closed orbit.

We now are in a position to compute the distinct properties of the electron and positron beams, and so we can at least in principle arrange the optical elements to minimize the differences. The most significant include differences in beam energies, damping times, and β^* .

Separated Orbits and Guide Field Errors. Of course our ability to compute and compensate effects of displaced orbits is ultimately limited by our knowledge of the details of the guide field. In particular, multipole errors can introduce peculiar effects in the company of separated orbits.

Quadrupole errors introduce a differential kick that can result in differential horizontal displacement of the beams at the interaction point with calamitous impact on luminosity. Elimination of such differences depends on a capability to reliably measure relative displacement of the beams. Generally the collinearity of the beams at the IP can be restored by a straightforward adjustment of the electrostatic separator voltages.

Skew quadrupole errors introduce a vertical kick that is proportional to the horizontal displacement of the closed orbit. The resulting vertical separation at the IP is similarly removed if vertical electrostatic deflectors are available. Lacking vertical deflectors there is no alternative but to use skew quadrupole trims to make corrections. This can prove a particularly unwieldy scenario. The skew fields couple horizontal and vertical oscillations. Skew quadrupoles located in regions where there is a large differential horizontal displacement will simultaneously effect both the vertical closed orbit and the vertical beam size. Optimization of luminosity depends critically on careful tuning of skew quadrupoles. In a machine with displaced orbits, tuning is greatly facilitated if there are skew quadrupoles located in regions where the orbits coincide.

3 Crossing Angle

In a multiple bunch scheme in which beams collide head on the collinearity through the interaction region is of great practical value. It permits a direct

determination of the relative displacement of the beams at the IP and provides a stretch of guide field in which skew quads can be implemented with abandon. But the collinearity ultimately limits spacing of the bunches in each beam. To be precise, if the collinear region extends a distance s from the IP then the distance between the bunches in each beam must be at least $2s$. Otherwise, the electrons and positrons will collide at the parasitic crossing point nearest the IP. We can accommodate beams with very closely spaced bunches in a single ring if we introduce a small horizontal crossing angle at the interaction point as shown in Figure 7. The crossing angle required to provide adequate separation at the

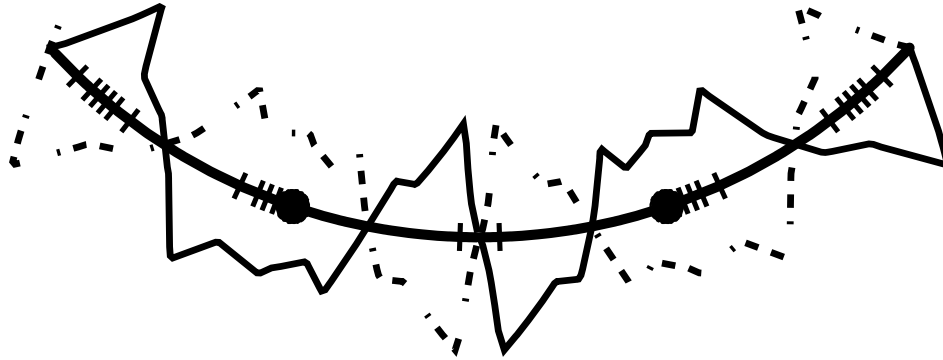


Fig. 7. Horizontal crossing angle at the interaction point. The electron positron crossing points are indicated by the tick marks along the central trajectory. Note the separation of the incoming positron(electron) bunch and the outgoing electron(positron) bunch on either side of the IP. The plot extends $\pm 100\text{m}$ on each side of the IP.

first parasitic crossing point depends in detail on the bunch spacing, and $\beta(s)$ in the interaction region. In typical low β optics with a bunch separation of 8 meters, a crossing half angle of $\theta_c \sim 2\text{mrad}$ is sufficient.

3.1 Dependence of Beam-Beam Tune Shift on Crossing Angle

With the introduction of the crossing angle the nonlinear beam-beam kick gains an additional dependence on the longitudinal displacement of the particle from the center of the bunch and a synchrotron coupling results. The effect of the coupling is characterized by the "badness" parameter $\kappa = \frac{\theta_c}{(\sigma_x/\sigma_z)}$ [P1]. Measurements at CESR indicate a soft dependence of the beam-beam tune shift

parameter on the crossing angle as shown in Figure 8. The implementation of a

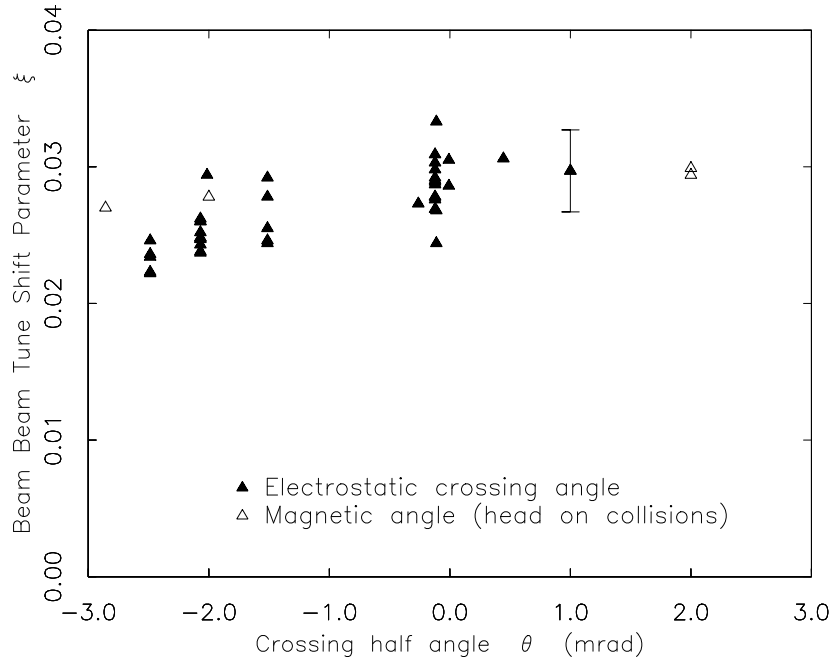


Fig. 8. The vertical tune-shift parameter as a function of crossing angle for average beam currents greater than $9ma/beam$. Open triangles are for head on collisions but with beams traversing the interaction point at the angle indicated. The open triangles thus give some notion of the effect of the large displacement in the IR optics.

crossing angle permits deployment of trains of closely spaced bunches. Just such a configuration is indicated in Figure 9.

The symmetries that characterize the operation of the "basic" collider have been all but abandoned in the interest of multiple bunches. There is no guarantee of equal tunes, beta functions, coupling, chromaticity or energy for the electron and positron beams. And there is no certainty the bunches will collide. Collisions are no longer head-on and there is no coincidence of trajectories anywhere in the machine. Except at nodes of the closed orbit distortion, skew quadrupole fields will displace the beams as well as change the aspect ratio. Of course all such effects can be corrected in principle with the help of suitable combinations of trim magnets. But the tuning by the accelerator operator that is such a critical aspect of performance, is enormously complicated, and good diagnostics become increasingly important.

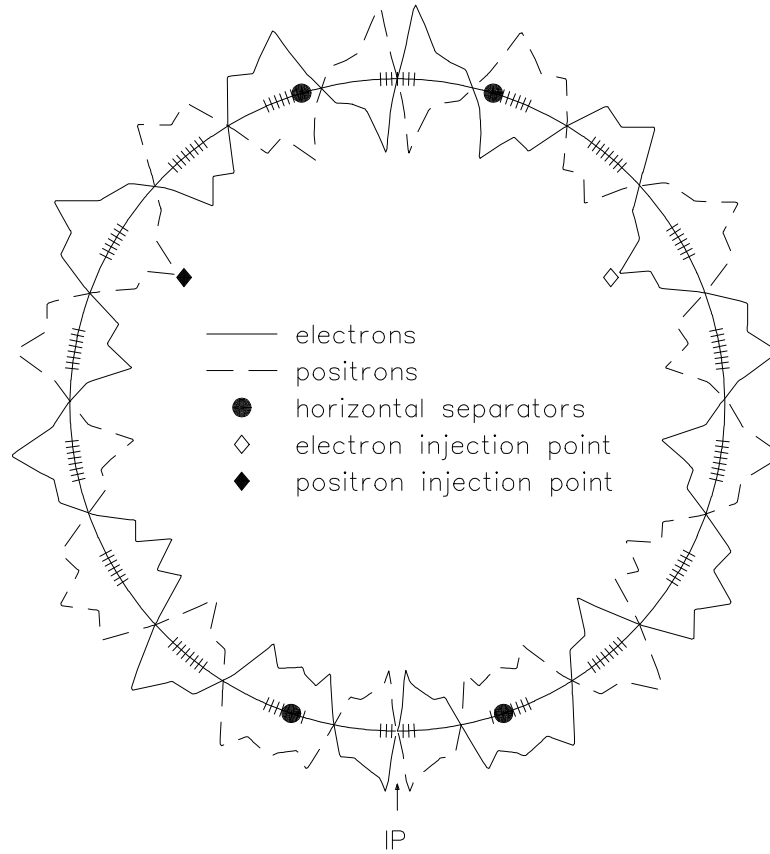


Fig. 9. The crossing angle at the IP is $\pm 2.1 \text{ mrad}$ and the peak horizontal displacement in the horizontally focusing interaction region quadrupole is about 2cm. The tick marks indicate the parasitic crossing points of the 9 trains of four bunches each. The bunches are spaced 4.2 meters apart within each train. Nine trains does not lend itself to equal spacings in CESR injector and storage ring, thus leading to the inconsistency in the number of crossing points from one lobe to the next.

3.2 Solenoid Compensation

Most collider detectors depend on the magnetic field of a solenoid in order to measure the momentum of the products of e^+e^- annihilation. The longitudinal field of the solenoid generates transverse coupling in the stored beams. As a beam particle traverses the radial fringe field of the solenoid it receives a transverse kick of amplitude proportional to its displacement from the magnet axis. It then follows a circular path about the longitudinal field, finally receiving a kick as it exits through the opposite fringe. Compensation of the transverse coupling is usually accomplished by a small rotation of the interaction region quadrupoles about the longitudinal axis. The rotation angles are chosen so that the mapping

of the transverse phase space through the compensation region to the interaction point is block diagonal. Then horizontal emittance does not contribute to vertical beam size at the interaction point. That is, if the transport through the region is described by

$$T = \begin{pmatrix} M & 0 \\ 0 & N \end{pmatrix}, \quad (55)$$

where M and N are 2×2 matrices, and

$$\begin{pmatrix} x \\ x' \\ y \\ y' \end{pmatrix}_{IP} = T \begin{pmatrix} x \\ x' \\ y \\ y' \end{pmatrix}_{outside} \quad (56)$$

then vertical motion at the collision point is decoupled from horizontal motion in the arcs. In addition, as long as the full turn matrix evaluated anywhere outside of the interaction region is block diagonal, there is no net or global coupling in the machine, and the transverse normal modes are horizontal and vertical. In the event of a small crossing angle at the interaction point, the solenoid field and its compensation gains considerable significance as we shall now see.

It is relatively easy to measure and therefore to correct global coupling. The most sensitive technique is to look for the minimum separation in normal mode tunes. But the local coupling, which determines the beam size at the interaction point, is accessible only by measuring the luminosity. It is therefore difficult to optimize operationally. So let us suppose for a moment that the machine is globally decoupled but that there is some error in the compensation. Then if the transfer matrix from outside the compensation region, through to the IP is

$$T = \begin{pmatrix} M & m \\ n & N \end{pmatrix} \quad (57)$$

with m and n , 2×2 nonzero matrices, the vertical beam size at the interaction point is proportional to the horizontal beam size outside of the compensation region, and the luminosity is diluted. If there is a horizontal crossing angle, the closed orbits of the two beams have equal but opposite displacement and angle as they enter the compensation region. And the displacement and angle can not both be zero or there will be no crossing angle. In particular

$$\begin{pmatrix} x \\ x' \end{pmatrix}_{start} \sim M^{-1} \begin{pmatrix} 0 \\ x' \end{pmatrix}_{IP} \quad (58)$$

and $x'_{IP} = \theta_c^*$. It follows that the difference in the *vertical* orbits at the IP is related to the difference in *horizontal* orbits at the start of the compensation region.

$$\begin{pmatrix} \Delta y \\ \Delta y' \end{pmatrix}_{IP} = n \begin{pmatrix} \Delta x \\ \Delta x' \end{pmatrix}_{start}. \quad (59)$$

In order to get some idea as to the size of such effects, suppose that the overall coupling of horizontal into vertical emittance is 1%. Now consider a 1%

compensation error. That is, the matrix n has some combination of values such that 1% of the horizontal emittance is added to the vertical emittance at the IP, effectively doubling it. The beam size at the IP grows by a factor of $\sqrt{2}$ and the luminosity similarly degraded. Meanwhile, the horizontal closed orbits of the two beams in the arcs are displaced an equivalent of $\sim 10\sigma_x$ in order that they be sufficiently well separated at the parasitic crossing points. The area in phase space bounded by the closed orbits of the two beams corresponds to an emittance about 100 times the horizontal emittance of a single beam since $\sigma_x \sim \sqrt{\epsilon_x \beta_x}$. The compensation error propagates 1% of that into the vertical at the IP leading to a vertical separation of $\Delta y \sim \sqrt{\beta_v \epsilon_x}$. The vertical beam size is already established to be $\sigma_y \sim \sqrt{0.01 \times 2 \times \epsilon_x \beta_y}$. The beams are thus separated by $\Delta y \sim 5\sqrt{2}\sigma_y$. We find that a compensation error that increases the beam size by 40%, results in a vertical separation in excess of $5\sigma_y$. The beams effectively miss each other. Evidently a compensation error that has a moderate effect on luminosity in terms of increased beam size, can have a devastating effect in terms of closed orbit errors.

4 Conclusion

The symmetry of Maxwell's equations with respect to time reversal guarantees that in machines in which guide fields are purely magnetic that orbits and twiss parameters be identical for both beams. But the basic e^+e^- collider has evolved to a multibunch machine with many more crossing points than collision points and the optics must be specifically constrained to preserve common beam properties. The successful operation of ever more complicated configurations depends critically on an ability to diagnose machine errors and the flexibility to correct them. This is especially true in the regime of very small β^* and totally distinct closed orbits.

References

- [SM1] Siemann, R., Meller, R.: Coherent Normal Modes of Colliding Beams, IEEE Trans. Nucl. Sci. **NS-28**, No. 3, 2431 (1981)
- [CS1] Courant, E.D., Snyder, H.S.: Theory of the Alternating Gradient Synchrotron, Ann. of Phys. **3**,1(1985)
- [CBW1] Chao, A.W., Bambade, P., Weng, W.T.: Nonlinear Beam-Beam Resonances. Nonlinear Dynamics Aspects of Particle Accelerators, Proceedings, Sardinia 1985, ed. J.Jowett, M.Month, S.Turner, 93-94
- [JS1] Seeman, J.: Observations of the Beam-Beam Interaction, Nonlinear Dynamics Aspects of Particle Accelerators, Proceedings, Sardinia 1985, ed. J.Jowett, M.Month, S.Turner, 126-137
- [P1] Piwinski, A.: Simulations of Crab Crossing in Storage Rings, SLAC-PUB-5430, February 1991
- [S1] Sands, M.: The Physics of Electron Storage Rings, SLAC-121, 1970, 100-102
- [SB1] Servranckx, R., Brown, K.: SLAC Report 270 UC-28 (A), March 1984
- [R1] Rubin, D.: Doubling the Damping Decrement in CESR, CON 87-12

- [RW] For a more complete treatment along these lines see Ruth, R., Weng W.: Physics of High Energy Particle Accelerators, AIP Conference Proceedings, No. 87 (1981), ed. R.Carrigan, F.Huson, M.Month, 4-16